Bioactive Materials 8 (2022) 396–408

Contents lists available at ScienceDirect

Bioactive Materials

journal homepage: www.sciencedirect.com/journal/bioactive-materials

Bioinspired supramolecular nanofiber hydrogel through self-assembly of biphenyl-tripeptide for tissue engineering

Yong Sun [a], Xing Li [a], Mingda Zhao [a], Yafang Chen [a], Yang Xu [a], Kefeng Wang [a], Shaoquan Bian [b,*], Qing Jiang [c], Yujiang Fan [a,**], Xingdong Zhang [a]

[a] National Engineering Research Center for Biomaterials, Sichuan University, 29 Wangjiang Road, Chengdu, Sichuan, 610064, PR China
[b] Shenzhen Institutes of Advanced Technology, Chinese Academy of Sciences, Shenzhen, 518055, PR China
[c] College of Materials Science and Engineering, Sichuan University, 29 Wangjiang Road, Chengdu, Sichuan, 610064, PR China

ARTICLE INFO

Keywords:
Supramolecular nanofiber hydrogel
Biphenyl-tripeptide self-assemblies
Molecular dynamics simulations
Hydrogen bond interactions
Cartilage tissue engineering

ABSTRACT

Supramolecular nanofiber peptide assemblies had been used to construct functional hydrogel biomaterials and achieved great progress. Here, a new class of biphenyl-tripeptides with different C-terminal amino acids sequences transposition were developed, which could self-assemble to form robust supramolecular nanofiber hydrogels from 0.7 to 13.8 kPa at ultra-low weight percent (about 0.27 wt%). Using molecular dynamics simulations to interrogate the physicochemical properties of designed biphenyl-tripeptide sequences in atomic detail, reasonable hydrogen bond interactions and "FF" brick (phenylalanine-phenylalanine) promoted the formation of supramolecular fibrous hydrogels. The biomechanical properties and intermolecular interactions were also analyzed by rheology and spectroscopy analysis to optimize amino acid sequence. Enhanced L929 cells adhesion and proliferation demonstrated good biocompatibility of the hydrogels. The storage modulus of BPAA-AFF with 10 nm nanofibers self-assembling was around 13.8 kPa, and the morphology was similar to natural extracellular matrix. These supramolecular nanofiber hydrogels could effectively support chondrocytes spreading and proliferation, and specifically enhance chondrogenic related genes expression and chondrogenic matrix secretion. Such biomimetic supramolecular short peptide biomaterials hold great potential in regenerative medicine as promising innovative matrices because of their simple and regular molecular structure and excellent biological performance.

1. Introduction

Functional hydrogels had achieved great progress in tissue regeneration since they simulate native extracellular matrix (ECM) [1–4]. Recently, more efforts were put on the development of fibrous hydrogels, expecting to acquire highly matched structures and functions with ECMs [5–7]. Collagen, which is the main component of ECM, consists of three long chains of amino acids spirally twisting in fibrous structure. It could promote cell adhesion, regulate cellular biofunctions and extracellular matrix formation. However, the complex production processes, expensive manufacturing cost, and immunogenicity due to its animal origin constrained its wide application [8–11]. Hence, it was of great challenge and significance to develop functionally biomimetic polypeptide. The synthetical polypeptides with nanofibrous structure had been reported to promote cell adhesion and regulate cell behaviors [12]. Meanwhile, the hydrogels modified or blended with functional polypeptide also enhanced its biological functions [13]. Nevertheless, the low synthetic efficiency, high minimum gelation concentrations (MGC), and multiphase composition increased the complexity of nanofibrous polypeptide. Hence, engineering-oriented simple and inexpensive polypeptide hydrogels, which were also responsive to cytocompatible stimuli such as pH or temperature and supportive to cells biofunction, were meaningful and urgent for tissue regeneration.

Stimuli-responsive supramolecular hydrogels were composed of building blocks based on fundamental biological molecules (e.g amino acids, saccharides and nucleobases) that assembled into higher order structures via noncovalent interactions, and had been used as excellent soft materials for cells culture [14,15], drug delivery [16], cancer

Peer review under responsibility of KeAi Communications Co., Ltd.
* Corresponding author.
** Corresponding author.
E-mail addresses: sq.bian@siat.ac.cn, sunyong8702@scu.edu.cn (S. Bian), fan_yujiang@scu.edu.cn (Y. Fan).

https://doi.org/10.1016/j.bioactmat.2021.05.054
Received 10 March 2021; Received in revised form 12 May 2021; Accepted 28 May 2021
Available online 11 June 2021

inhibition [17] and cellular imaging [18]. In particular, short peptides coupling series of hydrophobic functional molecules as low-molecular-weight gelators (LMWGs) were the most widely applicable motifs [15]. These functionalized short peptide gelators had arouse intensive interests owing to its advantages including simple and efficient synthetic route, similar fiber structure to native ECM, optimal biocompatibility without immunogenicity, and intelligent responsive behavior. Tanaka et al. reported a unique multicomponent hydrogel composed of a self-sorting double network prepared through a post-assembly fabrication protocol, which could respond to ATP and sarcosine through gel-sol transition behavior programmed in an AND logic gate fashion [19]. Wang et al. designed a series of peptides and demonstrated the insertion of an uncharged polar residue at the intramolecular hydrophobic/hydrophilic interface that promoted the formation of well-defined super-secondary structures based on side chain hydrogen bonding interactions among β-sheets [20]. Tan et al. used a biocompatible hydrogelator, Nap-Phe-Phe-Tyr-OH (NapFFY), to encapsulate SDF-1 and BMP-2 for the regeneration and reconstruction of periodontal bone tissues *in situ*. Nevertheless, the amino sequence dependent gelation behavior was rarely revealed, particularly on the factors dominating the sol-gel transformation [21].

We seek an approach to design peptide-based hydrogel using the power of computation to guide peptide engineering. Potential candidate peptides could be modeled in computational software, using molecular dynamics (MD) simulations to survey the physicochemical features of peptide system [22,23]. The novel computational approaches could help to design functional peptide scaffolds for tissue regeneration. It could also rapidly reveal the complex interactions between polypeptides and the solvents, as well as the stability of peptide molecules, which influenced their self-assemble capability. Herein, we integrated computational and experimental approaches in the design, synthesis, and characterization of a pH-triggered, self-assembling biphenyl-tripeptide as tissue engineering scaffold. To elucidate the self-assembly mechanism, we analyzed the influence of peptide sequences on self-assembly process, and key influencing factors were explored.

In this work, the diphenylalanine conjugated with 4-biphenylacetic acid (BPAA) was employed as a core segment to produce biphenyl-tripeptide compounds with different C-terminal amino acids, i.e. glycine (G), alanine (A) and phenylalanine (F). And then the alternative position of G and A in tripeptide sequence was carried out. For elucidating short peptide self-assembly processes, molecular dynamics (MD) simulations were employed to reveal structural properties and conformational dynamics of six short peptides by simulating multiple peptides aggregation in a single system. The biomechanical properties and intermolecular interactions were also analyzed by rheology and spectroscopy analysis to optimize amino acid sequence. Furthermore, the prospect of optimal nanofiber hydrogels to support chondrocyte proliferation and specific chondrogenic expression for *in vitro* cartilage tissue engineering by mimicking native extracellular matrix (ECM) was also investigated. The MD simulations combined with experimental verification provided a new strategy for optimally designing functional biomaterials for tissue regeneration applications.

2. Experimental section

2.1. Materials and methods

2-chlorotrityl chloride resin (100–200 mesh; 1% DVB; 1.01 mmol/g), Fmoc-L-Phe-OH, Fmoc-Gly-OH and Fmoc-L-Ala-OH were purchased from Shanghai GL biochem (China). DMEM, α-MEM medium and Phosphate Buffered Saline (PBS, 0.0067 M) were provided by Thermo Fisher Scientific Corporation (USA). Fetal bovine serum (FBS, Gibco, South America origin) was bought from Life Technologies Corporation (USA). All the other compounds were obtained by Chengdu Best-reagent Corporation (China) and used without further purification. ^{1}H NMR spectra were collected on a Bruker AVII-400 (400 MHz, USA) using DMSO-d_6 as a solvent. Liquid chromatography-mass spectrometry (LC-MS) analysis was performed on a Finnigan TSQ Quantum Ultra LC-MS system with an electrospray ionization (ESI) source.

2.2. Synthesis

The synthesis of 4-biphenylacetic acid conjugating tripeptide compounds (as BPAA-tripeptides for short) were presented by taking BPAA-FFG-OH as an example, which was produced following standard solid phase peptide synthesis (SPPS) using 2-chlorotrityl chloride resin (100–200 mesh and 1.01 mmol/g), Fmoc-Gly-OH and Fmoc-L-Phe-OH. Firstly, 2-chlorotrityl chloride resin (1.0 g, 1.0 mmol) was taken into the reaction vessel and swelled in dry dichloromethane (DCM) for 30 min. Then the solution containing the Fmoc-Gly-OH (357 mg, 1.2 mmol) and N, N-diisopropylethylamine (DIPEA, 420 μL, 2.4 mmol) in DCM was added and stirred for 1.5 h. After coupling reaction completed, the solvent was removed, and the resin was washed with DCM and quenched in a blocking solution (DCM/methanol/DIPEA = 7/2/1, v/v) for 10 min. Followed by washing with DMF, the amino acid loading resin was treated with 20% piperidine in DMF (v/v) for 30 min to remove the Fmoc-protecting group. Afterwards, the subsequent Fmoc-L-Phe-OH (581 mg, 1.5 mmol) in DMF was added and coupled to the amino acid loaded on the resin applying O-Benzotriazole-N, N, N′, N′-tetramethyl-uronium-hexafluor-ophosphate (HBTU, 570 mg, 1.5 mmol) and DIPEA (522 μL, 3.0 mmol) as coupling reagents. Then the coupling of the second Fmoc-L-Phe-OH and deprotecting of Fmoc group were repeated to elongate the peptide chain using the above method. Subsequently, a solution of 4-biphenylacetic acid (BPAA, 320 mg, 1.5 mmol), HBTU (570 mg, 1.5 mmol) and DIPEA (522 μL, 3.0 mmol) in DMF was added to react with the peptide chain. The resin was washed with DMF and DCM, and the compound was then cleaved from the resin using TFA/DCM (1:99, v/v). Finally, the resulting product was precipitated in cold diethylether, and analyzed by ^{1}H NMR and mass spectroscopy.

2.3. Hydrogel preparation

The synthesized BPAA-tripeptides were tested for gelation properties with concentration of 20 mM, 10 mM, 5 mM, 2 mM, 1 mM and 0.4 mM, respectively. To prepare aqueous solutions, compounds were initially suspended in 1 mL sterile deionized water and 1 M NaOH was added to increase the pH of the solutions to 9 by using a vortex. For the pH switch method, glucono-δ-lactone (GdL) was added to the solution and mixed completely to neutralize the NaOH and reduce the pH to 7. Afterwards, all the solutions were allowed to stand for about 24 h without disturbance, and the gel formation and gelation time was initially verified by tube inversion assay. For preparing hydrogels in simulated physiological condition (PC), 0.3 M PBS and GdL were added together, and the mixture solution were vortexed thoroughly to give a solution containing 0.01 M PBS with a final pH of ~7.0. Then the solution was left to form hydrogel.

2.4. Morphology of nanostructures

The morphology of the self-assembled nanostructures within the supramolecular hydrogels was observed using a TECNAI G2 F20 S-TWIN transmission electron microscope (TEM) operating at 200 kV, a HITACHI S-800 scanning electron microscope (SEM), respectively. To prepare samples for TEM study, the solution of gelator (10 μL) was dropped onto a carbon-coated copper grid (200 mesh), or the carbon-coated copper grid was inserted into the solution for 1 min. Then the samples on copper grids were negatively stained using phosphotungstic acid (10 μL, 2.0%) and air-dried in dust-free condition for 6 h. For SEM study, the samples were prepared by lyophilisation. Afterwards, the lyophilizate was further sputter-coated with a layer of gold to enhance the electrical conductibility.

2.5. Molecular dynamics simulations of tripeptides

All the BPAA-tripeptides models were constructed by the Visualizer of BIOVIA Discovery Studio 2019. The Dmol3 program in Materials Studio (Accelrys, San Diego, CA, USA) based on the quantum mechanics Density Functional Theory (DFT) was then adopted to optimize the structures of all synthetic molecule models. In the geometry optimization, the Perdew–Burke–Ernzerh (PBE) of generalized gradient approximation with the GGA density function was used to determine the exchange-correlation energy [37]. The DNP basis set was applied, which is comparable to the 6-31G basis set. The optimized eight individual molecules were solvated randomly in a water box with dimension of about 80 Å × 65 Å x 75 Å 150 mM Na^+ and Cl^- ions were also solvated in the final water box to neutralize the system charge. The whole systems containing BPAA-tripeptides have about 32000–35000 atoms. NAMD was adopted in all MD simulations [38]. The merged Charmm36_prot and Charmm36_cgenff force field was applied to describe the potential functions of BPAA-tripeptides [39]. The TIP3P water model was used for water box [40]. The long-ranged electrostatic force was calculated by the Particle-mesh Ewald summation, with a cutoff distance of 12.5 Å for the separation of the direct and reciprocal space. The van der Waals interactions were also truncated at 12.5 Å. All the systems were periodic in three (XYZ) dimensions. All the simulations executed a time step of a 2 fs in the NVT ensemble. A constant temperature of 310.6 K was managed in the simulations with the Langevin method. In order to obtain the relax geometry of molecules in water box, an energy minimization was firstly performed and a 1 ns MD relaxation with 1 fs time step was conducted to reach system equilibrium. After then, 100 ns MD simulation with all atoms mobile was carried out on the systems. For the simulation of micromolecules, tens of nanosecond simulations were considered satisfactory [41,42]. A numerical measurement of the Root Mean Squared Deviation (RMSD) was applied to evaluate the stability of the molecule clusters. It is defined as:

$$RMSD_\alpha(t_j) = \sqrt{\frac{\sum_{\alpha=1}^{N_\alpha}(\vec{r}_\alpha(t_j) - \vec{r}_\alpha)^2}{N_\alpha}}$$

where N_α is the number of atoms whose positions are being compared, $\vec{r}_\alpha(t_j)$ is the position of atom α at time t_j, and $\vec{r}_\alpha$is the average value of the position of atom α to which the position $\vec{r}_\alpha(t_j)$ are being compared. The second structures and the solvent accessible surface area (SASA) of the synthetic molecules were calculated by the timeline plugin of VMD. A self-written script of radius of gyration based on the theory was executed to describe the state of aggregation of molecules.

2.6. Rheology

The sol-gel transition was determined by a flow test utilizing a test tube inverting method reported by Jeong et al. [43]. The accurate gelation time and viscoelastic characteristics of the hydrogels were determined by rheology measurements on a TA Discovery DHR-2 rheometer with a parallel-plate geometry (40 mm) and a 1.0 mm gap. The time sweep in oscillation mode was operated with a constant ramp strain of 1% and frequency of 1 Hz. A combining measurement composed of "amplitude sweep" and "frequency sweep" was applied, and the dynamic amplitude sweep was operated with a log ramp amplitude ranging from 0.1% to 10% and a frequency of 1 Hz, which ensured the linear viscoelastic regime for dynamic frequency sweep. Then the elastic and viscous moduli were measured by using a log ramp frequency between 0.1 and 100 rad/s at a constant strain, which was chosen within the linear viscoelastic regime. Meanwhile, an integrated temperature controller was used to maintain the temperature at 25 °C. Afterwards, the time sweep was applied with a constant frequency of 1 Hz and two different amplitudes of 0.5% and 100% to detect the reversibility of the hydrogels.

2.7. Dynamic mechanical analysis

Dynamic mechanical analysis was performed to analyze the compressive mechanical properties of hydrogels. The storage modulus (G′) and loss modulus (G″) of the hydrogels were determined by a Dynamic Mechanical Analyzer (DMA, TA-Q800, USA) instrument in the multi-frequency mode with a fixed frequency of 1, 2, 5 and 10 Hz at constant room temperature. The testing parameters were set at an amplitude of 40 mm, a preload force of 0.001 N and a force track of 105%. Every sample was measured in triplicate.

2.8. Environmental-responsive test

The environmental-responsive tests for four hydrogels (BPAA-AFF, BPAA-FFA, BPAA-GFF and BPAA-FFG) were performed in PBS (0.01 M) solution to investigate swelling and degradation behavior of these hydrogels. The prepared disc-shaped hydrogels were weighed (Wo). And then, they were immersed into 0.01 M PBS solution in a constant temperature shaker at 90 rpm at 37 °C. At a certain time interval, the hydrogels were taken out and wiped using filter paper to remove surface water, then they were weighed again (Wr). Every sample was measured in triplicate. The mass fold change of hydrogels was calculated as follows: Mass fold change = Wr/Wo.

2.9. Small angle X-ray scattering experiments (SAXS)

The SAXS experiments were performed on SAXS ess mc2(Anton Paar, Austria); the incident X-ray wavelength was 1.54 Å; the distance from sample to detector was 1590 mm; the ambient temperature was 27 °C.

2.10. CD, FTIR and fluorescence emission measurements

CD spectra were tested using an Applied Photophysics Chirascan Circular Dichroic spectrometer. The solution of gelators or hydrogels were added into a 3 mL quartz cuvette, and the data were recorded with a bandwidth of 1 nm, a step of 1 nm, a collection time of 0.5 s per point and a range of wavelengths between 190 and 350 nm. FTIR spectra were collected on a Thermo Scientific Nicolet 6700 FTIR at 2 cm^{-1} resolution. Hydrogels were prepared as described above, then the gelators and hydrogels were frozen in liquid N_2 and lyophilized. For the measurements, the KBr disk technique was used. Fluorescence emission spectra were detected on a Hitachi F-7000 Fluorescence Spectrophotometer. The solution of gelators or hydrogels were also placed into a quartz cuvette, and the data were collected with an excitation wavelength of 265 nm, bandwidth of 1 nm and a range of wavelengths between 250 and 500 nm at room temperature. All measurements were repeated three times and averaged into a single plot.

2.11. Cytotoxicity measurements

MTT experiments were conducted to evaluate the cytotoxicity of gelators on L929 cells. L929 cells were cultured using standard procedures in DMEM (10% FBS) and subsequently suspended and placed into a 96-well plate with a concentration of 2000 cells per well, followed by adhering for 12 h in incubator (37 °C, 0.5% CO_2). Meanwhile, the gelators were dissolved in H_2O and then diluted with cells culture medium, producing the treatments with gradient concentrations. Afterwards, cells culture medium was removed from the wells and replaced by the treatments, and wells treated with only DMEM (10% FBS) was regarded as control. Following the cells incubation for 24 h, 48 h and 72 h, MTT solution (20 μL, 0.5%, w/v) was added into the wells to replace the culture medium and the cell culture plates were left to incubate for 4 h (37 °C). Afterwards, the solution was removed and DMSO was added to dissolve the formed formazan. Finally, the absorbance was measured using a Thermo Scientific Varioskan Flash Multiscan Spectrum at the wavelength of 490 nm and the data was processed using Excel software.

The cytotoxicity of gelators against chondrocytes were evaluated following the same method, while chondrocytes were cultured in α-MEM (10% FBS).

2.12. Cell co-culture with BPAA-tripeptide hydrogels

L929 cells within culture dishes were trypsinized using trypsin (0.25%)-EDTA solution and suspended in cell culture medium (DMEM + 10% FBS). For 3D-culture, the gelation of supramolecular BPAA-tripeptide was carried out through pH switch (GdL), in which the resulting salt concentration was 0.01 M and pH value was 7.0 (similar to physiological condition). Then, the gelator solutions were immediately mixed well with L929 cells suspension to reach a final concentration of 2 $\times 10^6$ cells/mL, and the mixture was left for 30 min in molds to achieve the gelation. Afterwards, the cell-gel constructs were incubated for 7 days and the cell culture media were exchanged daily. The 3D culture of chondrocytes was conducted following the same process. In contrast, chondrocytes were cultured in α-MEM (10% FBS) with a final concentration of 5 $\times$ 10^6 cells/mL, and the cell-gel constructs were incubated for 21 days. Live/dead assays were used after incubation. Firstly, the cell-hydrogel constructs were swelled in PBS to wash the medium. Then the cell-hydrogel constructs were emerged in freshly prepared live/dead stain containing FDA (live, green, Ex = 488 nm, Em = 530 nm) and PI (dead, red, Ex = 535 nm, Em = 615 nm) for 1 min to stain the cells. Subsequently, the stained cell-hydrogel constructs were swelled in PBS again to wash the excess FDA/PI staining. The additional cytoskeletal F-

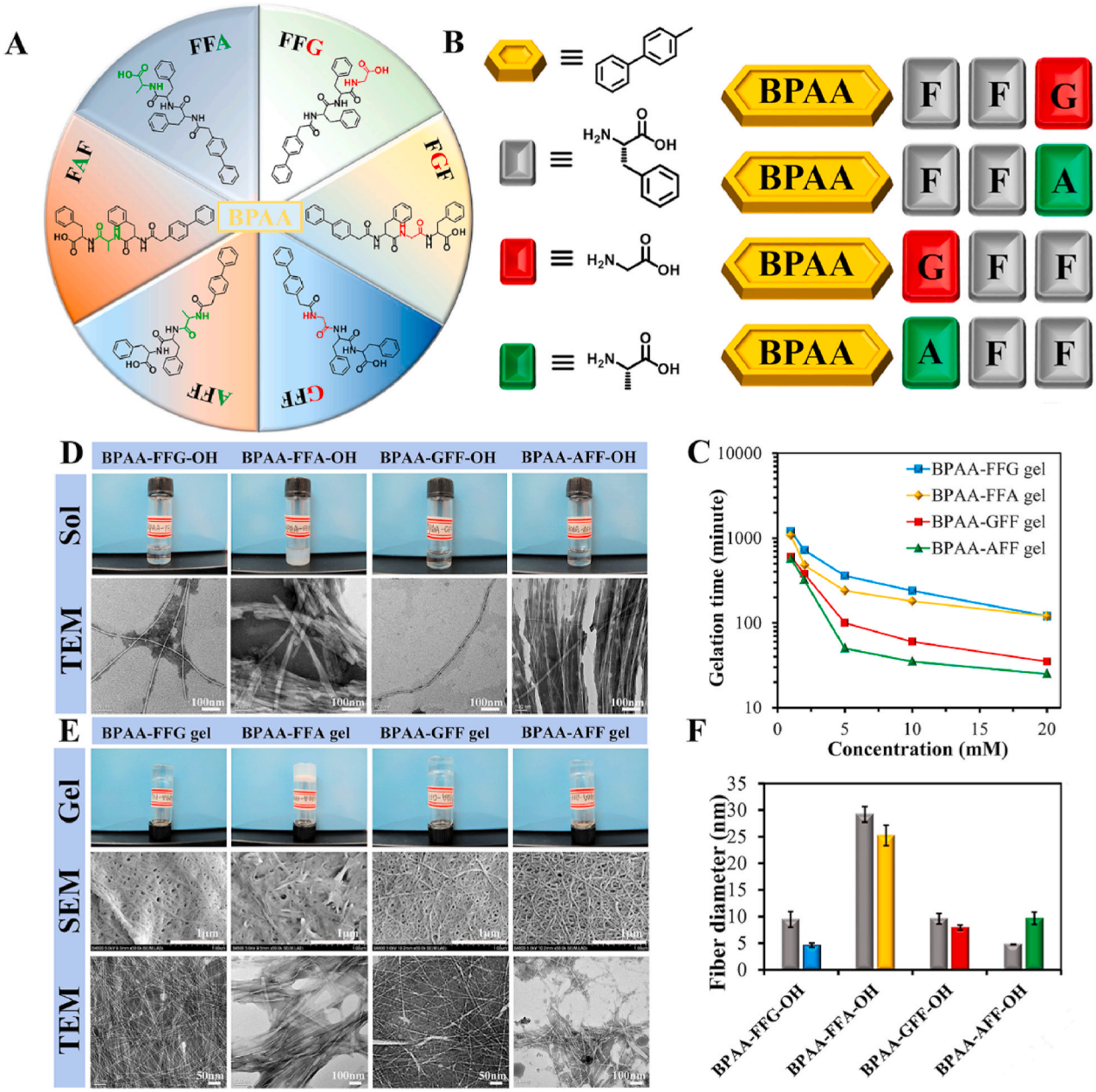

Fig. 1. (A) Chemical structures of BPAA-tripeptide compounds. (B) Four sequences that could form hydrogel via PH switch. (C) The gelation time of four sequences peptides with gradient concentrations. (D) The optical images and transmission electron micrograph (TEM) images of BPAA-FFG-OH solution (5 mM/0.27 wt %), BPAA-FFA-OH solution (5 mM/0.28 wt%), BPAA-GFF-OH solution (5 mM/0.27 wt %) and BPAA-AFF-OH solution (5 mM/0.28 wt%) at pH = 9. (E) The optical images, scanning electron micrograph (SEM) and transmission electron micrograph (TEM) images of BPAA-FFG-OH hydrogel (5 mM/0.27 wt %), BPAA-FFA-OH hydrogel (5 mM/0.28 wt%), BPAA-GFF-OH hydrogel (5 mM/0.27 wt %) and BPAA-AFF-OH hydrogel (5 mM/0.28 wt%) formed at pH = 7. (F) Fiber diameter analysis of four peptides before and after gelation.

actin stain were performed by using rhodamine-phalloidin (red, Ex = 545 nm, Em = 570 nm) and Hoechst 33342 (blue, Ex = 350 nm, Em = 460 nm) after incubation for 7 days. Firstly, the cell-hydrogel constructs were swelled in PBS to wash the medium. Secondly, the cell-hydrogel constructs were treated with 4.0% formaldehyde to fixed cells. Thirdly, the cell-hydrogel constructs were emerged in rhodamine-phalloidin staining for 40 min to stain the cytoskeletal F-actin of cells. Then the cell-hydrogel constructs were emerged in DAPI staining for 1 min to stain the cell nucleus. Subsequently, the stained cell-hydrogel constructs were swelled in PBS again to wash the excess rhodamine-phalloidin/Hoechst 33342. After staining, the fluorescent pictures of L929 cells were taken on a Leica TCS SP5 confocal laser scanning microscope (CLSM). The 3D culture of chondrocytes was conducted and the morphology of chondrocytes was observed following the same process. In contrast, chondrocytes were cultured in α-MEM (10% FBS) with a final concentration of 5×10^6 cells/mL, and the cell-gel constructs were incubated for 21 days.

2.13. Data analysis

All data were presented as mean ± standard deviation (SD). Statistical analysis was performed using SPSS version 15.0 software (SPSS Inc., Chicago, USA). The statistical differences were analyzed by one-way analysis of variance (ANOVA) with post hoc tests. A p value of <0.05 was considered statistically significant.

3. Results and discussion

3.1. The design and optimization of BPAA-tripeptides

The BPAA-tripeptides were synthesized by standard solid phase peptide synthesis (SPPS) using 2-chlorotrityl chloride resin and Fmoc protecting amino acids (Figure S1). Glycine and alanine as two hydrophilic amino were designed and coupled with FF dipeptide to generate six tripeptides with transforming amino sequence, they were components of collagen amino acid sequences, and its hydrophilicity was conducive to balance the hydrophobic properties of FF segment and enhance the affinity of cells. Their chemical structures (Fig. 1A) were analyzed by ^{1}H NMR spectrum and ESI-MS, and listed in Supporting **Information** along with the yields. As shown in Fig. 1A, all kinds of BPAA-tripeptides possessed a carboxylic acid terminal. The addition of NaOH solution or increase of medium pH would result in deprotonation of the terminal carboxylic acid and successful dissolution of the BPAA–tripeptide compounds. After adding to the basic solution, GdL (delta-Gluconolactone) was hydrolyzed to form gluconic acid and neutralize NaOH, and protonated the terminal carboxylic acid [24], leading to the self-assembly of molecules to form supramolecular hydrogels at pH = 7. The gelation properties of BPAA-tripeptides under switched pH treatment were shown in Table 1. Four sequences could form hydrogels, and were exhibited in Fig. 1B. BPAA-FFG and BPAA-FFA gelators could form homogeneous hydrogels triggered by decreasing pH; BPAA-GFF and BPAA-AFF could form homogeneous and transparent hydrogel. The other two BPAA-tripeptides, BPAA-FGF and BPAA-FAF, just formed white precipitations. For aromatic short peptide gelators, the tiny change in chemical composition of short peptides always led to distinct different self-assembly behaviors [25]. It was possible that the specific amino acid sequence of GFF and AFF could separate the phenylalanine and biphenyl group and decrease the steric hindrance, provide enough rotation space for biphenyl group to reach an appropriate position and produce a stable supramolecular arrangement. Another probable reason was that the diphenylalanine sequence could supply enough π-π stacking interactions for BPAA-GFF and BPAA-AFF to self-assemble into three dimensional networks, while the two separated phenylalanine didn't have the same function, which illustrated the crucial role of FF sequence in the design of aromatic short-peptide gelators. Furthermore, all the four hydrogels had quiet low minimum gelation concentrations (MGC) of about 0.4 mM or 0.022 wt%, corresponding to the water content of about 99.98 wt%. The gelation time of the hydrogels highly depended on the gelators concentration as shown in Fig. 1C in detail, which was determined by rheology measurements. The gelation time decreased from FFG to AFF might attribute to the methyl group on the alanine residue of BPAA-AFF and BPAA-FFA, which could decrease the flexibility of biphenyl-tripeptides moiety and reduce conformational entropy of the molecules [44]. Besides, the alanine or glycine between BPAA and FF blocks could separate the π electron spatial distribution, facilitating more π-π stacking formation [45]. The superior gelation properties compared with traditional macromolecular hydrogels provided high potential for biomedical application.

Table 1
Gelation properties of BPAA–tripeptide compounds.

Entry	Compound	Dissolve: pH = 9 [a]	Treatment: pH switch [b]	MGC (mM/wt%)	Gelation time [c]v (hour)
1	BPAA-FFG-OH	Clear solution	Transparent hydrogel	0.4/0.022	24
2	BPAA-FFA-OH	Semi-clear solution	Semi-transparent hydrogel	0.4/0.023	24
3	BPAA-FGF-OH	Clear solution	Precipitation	n/a	n/a
4	BPAA-FAF-OH	Clear solution	Precipitation	n/a	n/a
5	BPAA-GFF-OH	Clear solution	Transparent hydrogel	0.4/0.022	12
6	BPAA-AFF-OH	Clear solution	Transparent hydrogel	0.4/0.023	12

[a] : Adding 1.1 equiv. NaOH compared to the compound.

[b] : Adding GdL to neutralize NaOH.

[c] : Gelation time at MGC.

3.2. Guided nanostructure of self-assembled short-peptides by amino acid sequence transposition

The amino acid sequence in aromatic short-peptide gelators had great influence on their self-assembly behaviors [26,27]. Multiple measurement methods were employed to analyze the phenomenon. Transmission electron microscopy (TEM) and scanning electron microscopy (SEM) were used to reveal the morphology of nanostructures in the hydrogels (Fig. 1D and E), and the width of nanofibers were quantified as shown in Fig. 1F. At pH = 9, the long and worm-like nanofibers were observed for BPAA-FFG, BPAA-GFF and BPAA-AFF solution by TEM, while BPAA-FFA in basic solution aggregated into short-bar-shaped fiber bundle. The Gel-FFG, Gel-GFF and Gel-AFF formed at pH = 7 was homogeneous and transparent, while Gel-FFA was white semi-transparent. The TEM micrographs showed that Gel-FFG, Gel-GFF and Gel-AFF were composed of nanofibers with regular widths of 4 nm, 8 nm and 10 nm, respectively. It was worth noting that the obviously bundles aggregated by several paralleled nanofibers can be observed in Gel-FFG. However, the significantly different morphology was found in Gel-FFA, which was composed of overlapped short nanoribbons with widths varied from 23 to 28 nm. Nanofibers and bundles entangled with a high density, and short nanoribbons derived from short-bar-shaped fiber overlapped and crosslinked with a high density, which aroused a higher crosslinking density than that of Gel-FFG, and might lead to form a relatively stiffer hydrogel. The SEM micrographs showed that the nanofibers within Gel-FFG, Gel-GFF and Gel-AFF had a regular size and contacted with each other closely. By contrast, the short nanoribbons with random arrangement could be observed in Gel-FFA. These results were corresponding to the micrographs of TEM.

3.3. Conformational dynamics and interaction features via MD simulations

For elucidating short peptide self-assembly processes, MD simulations were used to examine structural properties and conformational dynamics of six short peptides by simulating multiple peptides aggregation in a single system. Six biphenyl-tripeptide assemblies was experimentally established in aqueous media to probe structural features in self-assembly process within 100 ns (Fig. 2 and Figure S2). The results showed that all biphenyl-tripeptide assemblies primarily exhibited irregular conformations (Fig. 2A) and formed an aggregates with 7 molecules in 100 ns (Fig. 2B). However, the number of aggregated molecules in simulation process was variant. BPAA-AFF, BPAA-GFF and BPAA-FFG could assemble quickly into a single aggregate at 50 ns, while other biphenyl-tripeptides appeared distinct double aggregates, even three aggregates in BPAA-FFA. Following the analysis results of Fig. 1, the sequences logo revealed that the "FF" brick was crucial for hydrogel formation (Fig. 3A) [28,29]. Hence, rapid formation of single aggregates was essential for the formation of stable fibrous gels. Noteablely, BPAA-FFA short peptides assembled into semi-transparent hydrogel (Fig. 1D and E) and presented significantly thicker fiber diameter (Fig. 1F). Combined with abnormal three aggregates formation at 50 ns in MD simulations (Fig. 2B), we speculated that polyaggregate structure of BPAA-FFA made peptides molecule tend to precipitation, but the binding of FF mitigated this tendency to a large extent, so that the semi-gel state with coarse nanofibers was presented.

Considering that interactions between peptide molecules and water were crucial for the conformational dynamics of supermolecular peptides system, we quantified the solvent-accessible surface area (SASA) of individual residues in each biphenyl-tripeptide, averaged over entire 100 ns trajectories (Figure S3). The biphenyl-tripeptide sequences containing Gly were more exposed to water than those containing Ala. However, no significant difference was observed among six peptide assemblies. On the other hand, the hydrogen bond intensity was also a major factor on regulating biphenyl-tripeptide structures. Thus, the number of intramolecular hydrogen bond was examined. At the end of simulation, the number of intramolecular hydrogen bond in BPAA-FAF and BPAA-FGF was more abundant in relative to other sequences (Fig. 3B and Figure S4). The excessive intramolecular hydrogen bond could impede the formation of intermolecular hydrogen bond, thus induce compact aggregates and precipitation. Then, we examined the time-evolution of the radius of gyration (R_g) of peptide systems. It reflected the rearrangement from diffuse peptide system to closely connected aggregates. As indicated by the tendency of R_g for biphenyl-tripeptide sequences relative to simulation trajectory (Fig. 3C), BPAA-FAF and BPAA-FGF peptide systems exhibited higher assembly propensity with obviously reduced R_g. For other four sequences, the dynamic change between aggregation and dissociation occurred during the simulation and the R_g was higher at the end of the simulation, related to the beginning of trajectory, indicating that transformation of peptides system was more kinetically allowed, i.e. transitions between secondary structures and transform balance between sol-gel. These data were consistent with the above detection of hydrogen bond among simulation process. In order to further evaluate the stability of peptide cluster during last 20 ns simulation, Root Mean Square Deviation (RMSD) was referenced to estimate the sequences regulating performance (Fig. 3D). Accordantly, the results showed that the largest cluster in BPAA-FAF and BPAA-FGF peptides system was stable at the end of simulation process; other four sequences exhibited a dynamic evolution along with simulation. All these results indicated that BPAA-FAF and BPAA-FGF could result in precipitation due to excessive intramolecular hydrogen bond.

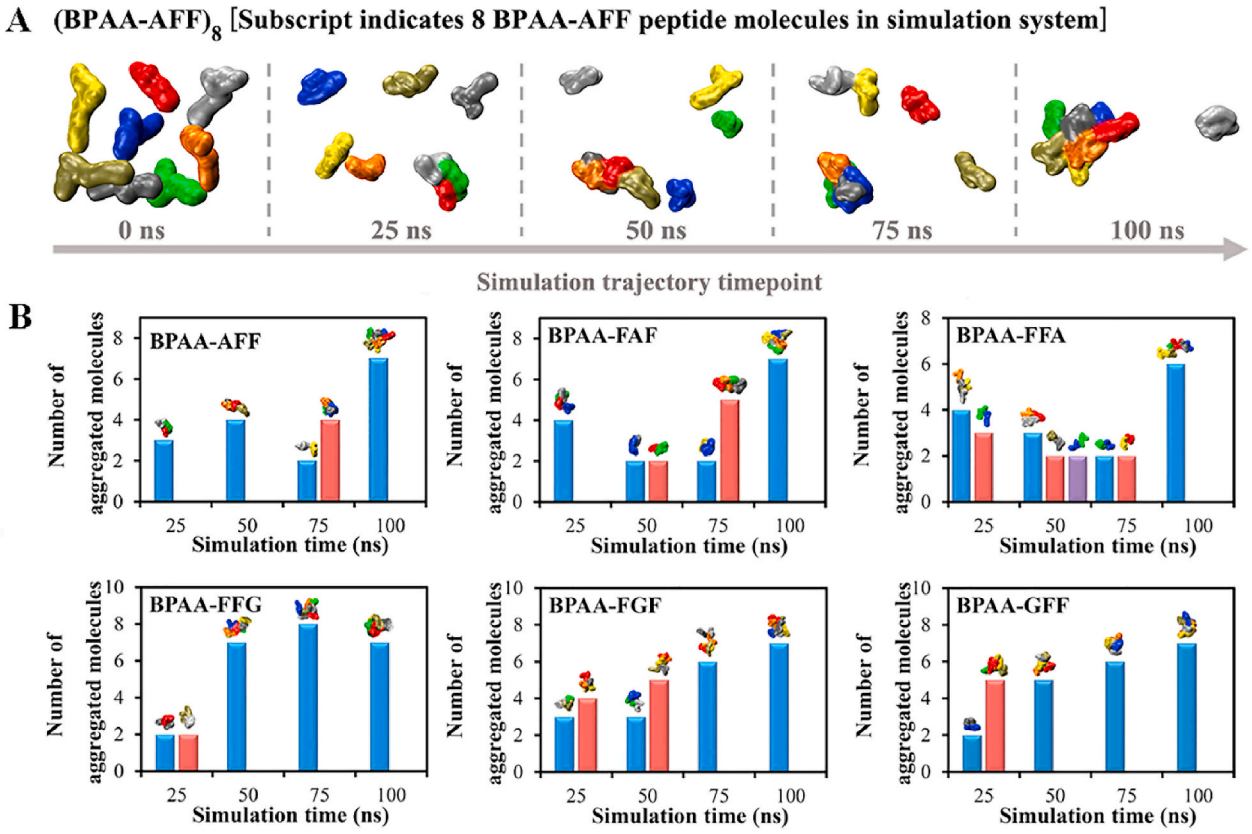

Fig. 2. Six divergent peptide molecules simulated in water solvent assembled into multimeric structures. (A) Conformation evolution of eight BPAA-AFF molecules was demonstrated as the peptides molecules gradually assembled into large clusters from 25 ns to 100 ns. (B) The number of aggregated molecules analysis during the 100 ns simulation with representative snapshots of the peptides molecules.

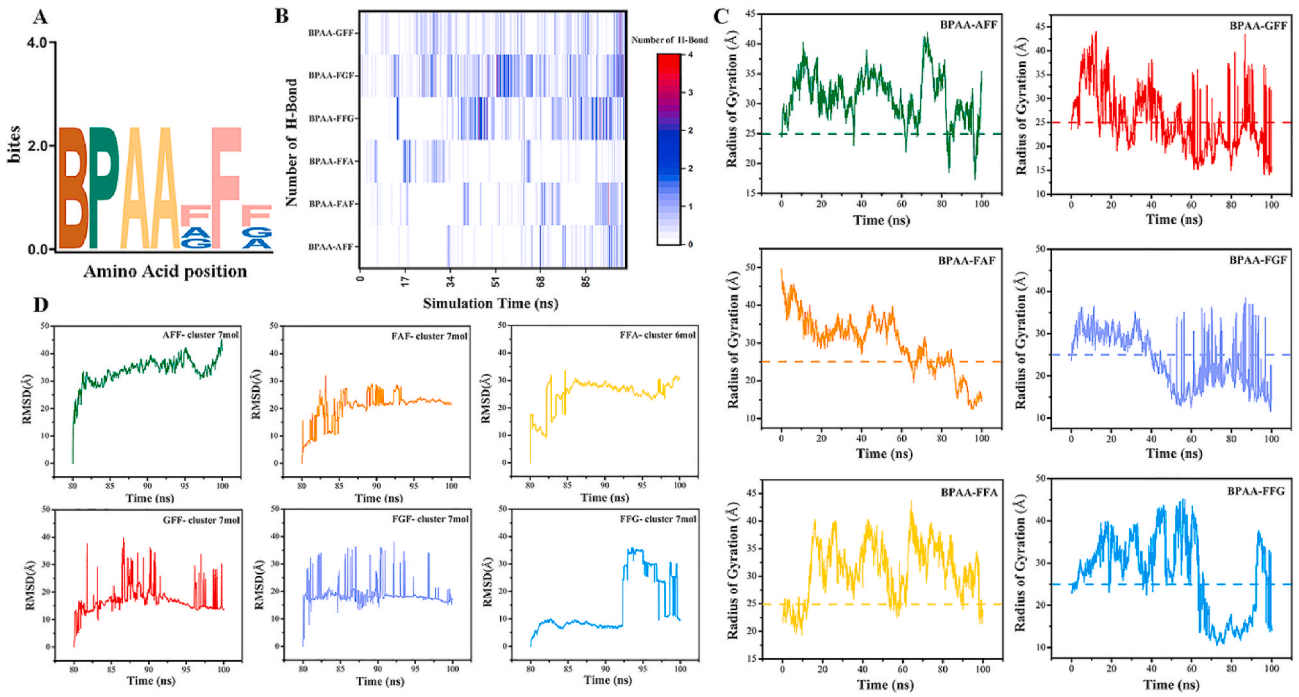

Fig. 3. (A) Sequence logo indicating that crucial effect of the di-phenylalanine (FF) in guiding hydrogel formation. (B) Heatmap of intramolecular hydrogen bond during simulation process. (C) Sequence dependence of the radius of gyration (R_g). Dashed line indicates initial R_g before equilibration. (D) Root mean square deviation (RMSD) evaluation at the end of 20 ns simulation.

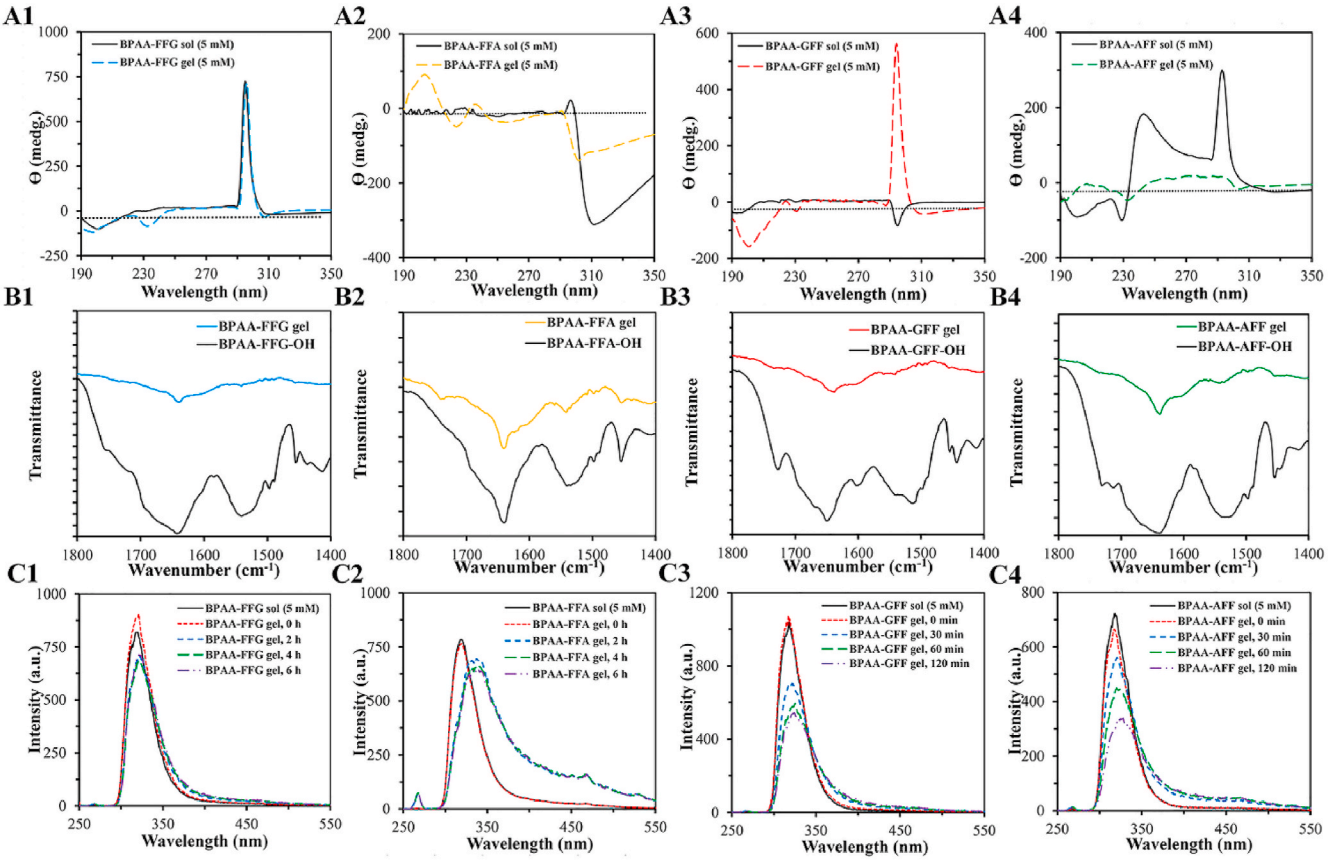

Fig. 4. (A1-A4) CD spectra of Sol-FFG, Sol-FFA, Sol-GFF, Sol-AFF and Gel-FFG, Gel-FFA, Gel-GFF, Gel-AFF. (B1–B4) FT-IR spectra of Gel-FFG, Gel-FFA, Gel-GFF and Gel-AFF. (C1–C4) Fluorescence emission spectra of Sol-FFG, Sol-FFA, Sol-GFF and Sol-AFF before and after addition of GdL. (λexc = 265 nm).

3.4. Secondary structure and intermolecular arrangement via CD, FTIR and fluorescence emission spectroscopy analysis

The secondary structure of the supramolecular architecture was investigated using circular dichrosim (CD) spectra and Fourier transform infrared (FT-IR) spectroscopy. The data of CD spectra (Fig. 4A1-A4) revealed that the supramolecular polymers generated by gelators at pH = 7 presented the typical β-sheet self-assemble structure, which was consistent with the results of MD simulation. Taking the CD spectra of Gel-FFG as an example, the two weak negative signals in the range of 190–215 and 225–235 nm (n-π* transition) indicated that the gelators predominantly arranged in a β-sheet conformation [30]. Moreover, the signal between 290 and 305 nm (π-π* transition) confirmed the superhelical arrangement of the biphenyl groups. In particular, the CD spectra of Sol-AFF showed nearly a linear plot close to the X axis, which indicated that the solution was probably composed of the monomers or small aggregates, such as micelles or vesicles [31]. Furthermore, all the FT-IR spectra of gelators (Fig. 4B1-B4) showed a strong C═O stretching peak at 1643 cm^{-1}, while the C═O stretching peak shifted to 1639 cm^{-1} for all the hydrogels, indicating the formation of typical β-sheet structure [32,33].

The fluorescence emission spectroscopy (Fig. 4C1-C4) was used to analyze the intermolecular arrangement of gelators along the time after adjusting the pH to 7 with GdL. It was worth mentioning that the emission spectra after adding GdL exhibited nearly similar graph with time extension, indicating weak molecular interactions in BPAA-FAF and BPAA-FGF solutions (Figure S5A, B). The fluorescence emission spectra of Sol-FFG and Sol-GFF showed a shark signal with a peak at 319 and 318 nm, respectively, while the emission spectra after just adding GdL exhibited nearly a same graph with a bigger value as shown inFig. 4C1 and 4C3. With the time extension, the sharp signal of the emission spectra exhibited a slight red shift from 318 to 325 nm, indicating the overlap of biphenyl groups in an antiparallel manner [34]. Furthermore, a broad phosphorescence peak centered around 400 nm appeared after adjusting the pH to 7, which arose from extensive π-π stacking [35,36]. The similar phenomenon was also discovered in Sol-AFF (Fig. 4C4). It was noteworthy that the fluorescence emission spectra of Sol-FFA (Fig. 4C2) presented more obvious red shift from 318 to 343 nm, which indicated the overlap of biphenyl groups in an antiparallel manner. Meanwhile, stronger phosphorescence peak disclosed a more extensive π-π stacking. These results showed that the gelators in Gel-FFA could possess stronger molecular interactions, constructed more stable supramolecular arrangements and generated stiffer hydrogels. Moreover, the phosphorescence signals of Gel-AFF were stronger

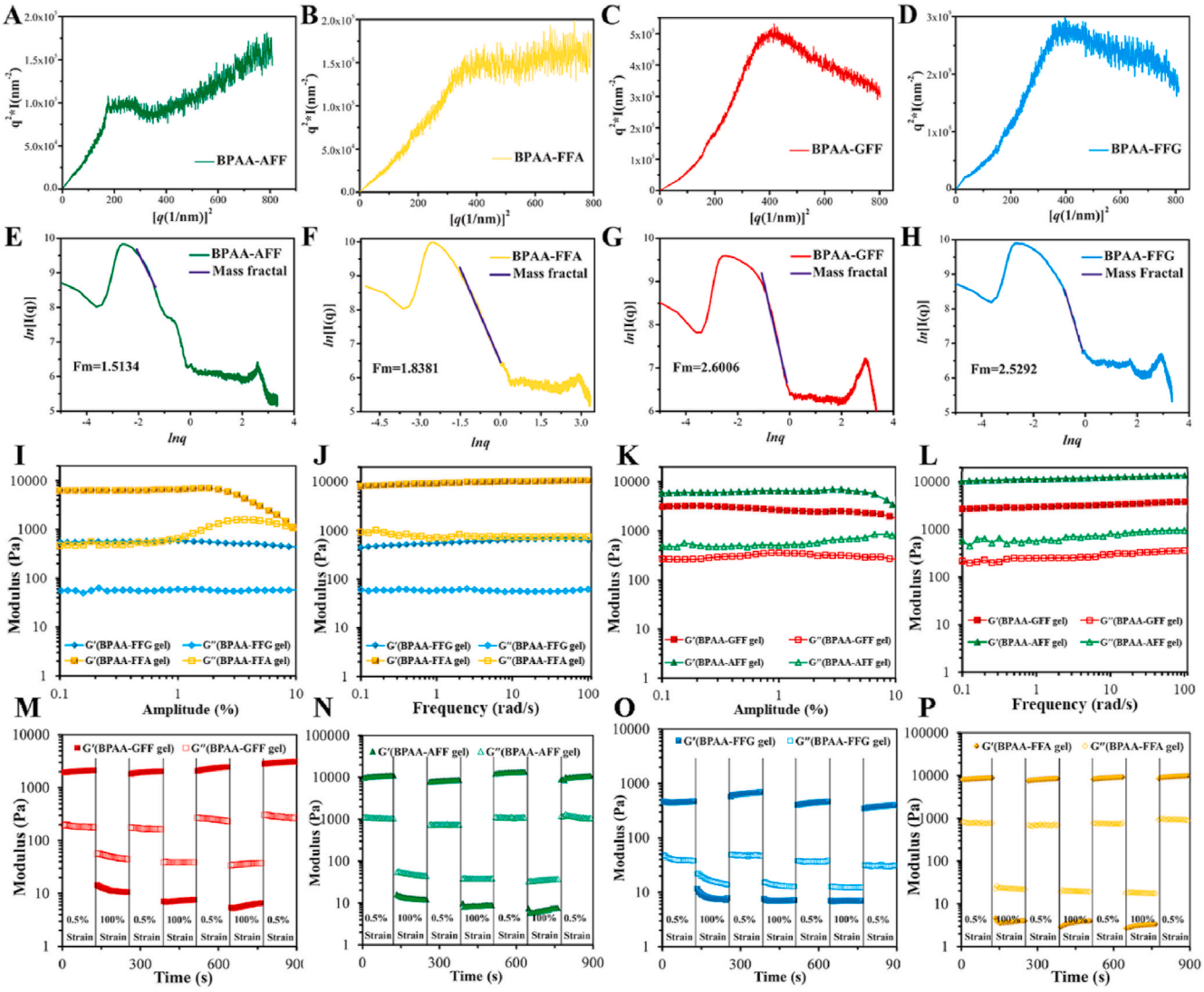

Fig. 5. (A–D) Kratky plots of the SAXS data. (E–H) Fractal dimension analysis. (I and K) Amplitude sweep analysis of hydrogels (Frequency = 1.0 Hz). (J and L) Frequency sweep analysis of hydrogels (Strain = 0.5%). (M − P) Time sweep analysis of hydrogels (Strain = 0.5% or 100%). Gel-GFF = 5 mM/0.27 wt%, Gel-AFF = 5 mM/0.28 wt%, Gel-FFG = 5 mM/0.27 wt%, Gel-FFA = 5 mM/0.28 wt%.

than that of Gel-GFF. The result showed that the Gel-AFF could have better mechanical properties. The environmental-responsive tests for four hydrogels (BPAA-AFF, BPAA-FFA, BPAA-GFF and BPAA-FFG) were performed in PBS (0.01 M) solution to investigate swelling and degradation behavior of these hydrogels (Figure S6). The BPAA-AFF possessed a moderate degradation behavior, indicating more stable molecular structure.

3.5. Conformational difference and mechanical property analysis of hydrogels via SAXS experiment and rheological test

SAXS experiments were carried out to probe conformational difference, the Kratky curves were shown in Fig. 5A–D. An obvious peak followed by rising to a plateau was found in BPAA-AFF, indicating the combination of folded conformation and random coil. BPAA-FFA also showed a dispersive long chain structure. However, a distinct peak was found in BPAA-GFF and BPAA-FFG hydrogels, which implied a compact conformation of molecular chains [46,47]. By comparison, the Kratky plot of four hydrogels illustrated two different profile, which confirmed the glycine and alanine as two dominant amino could affect conformational behavior of hydrogels. Fractal theory was adopted for analyzing the structural aggregates [48], the results were shown in Fig. 5E–H. Fractal dimension increased from 1.5134 for BPAA-AFF to 2.5292 for BPAA-FFG. The increasing fractal dimension implied the hydrogels with glycine displayed more disordered mass distribution, which could lead to unstable structure of hydrogels. Rheology measurements were used to characterize the viscoelastic properties of the hydrogels. An amplitude sweep analysis (Fig. 5I and **K**) was performed to confirm that the measurements were in the linear viscoelastic regime ($G' > G''$) within the range from 0.1 to 10% for Gel-FFG, Gel-FFA, Gel-GFF and Gel-AFF. Compared with Gel-FFG and Gel-GFF, the strain behavior of Gel-FFA and Gel-AFF could be classified as weak-strain overshoot, whose elastic modulus (G') decreased with increasing amplitude, but the viscous modulus (G'') firstly rose before slightly descent when the value of amplitude was more than 1%. For frequency sweep analysis (Fig. 5J and **L**), the value of amplitude was chosen as 0.5% within the linear viscoelastic regime, and the oscillating rheometrical data of the hydrogels showed that the value of elastic modulus G' was higher than that of viscous modulus G'', indicating effective hydrogels formation. All these hydrogels prepared by pH switch presented weak frequency dependence when the value of amplitude was chosen as 0.5%. The G' of Gel-FFG, Gel-FFA, Gel-GFF and Gel-AFF was around 0.7, 7, 4 and 13.8 kPa, respectively, which agreed well with the rheological characteristics of hydrogels. The methyl group on the alanine residue of Gel-AFF could decrease the flexibility of biphenyl-tripeptides moiety and reduce conformational entropy of the molecules, which was conducive to form a more stability hydrogel and acquired a higher elastic modulus. The time sweep analysis at room temperature (Fig. 5M–P) showed the gel state ($G' > G''$) at 0.5% amplitude and the liquid state ($G' < G''$) at 100.0% amplitude of the hydrogels, which revealed the reversibility of hydrogels.

3.6. Influence of amino acid sequence transposition on biological performance

Fig. 6A1-A2 showed the optical images and SEM micrographs of the hydrogels prepared in simulated physiological condition (PC) (pH = 7 and 0.01 M PBS). Hydrogels prepared by BPAA-GFF and BPAA-AFF under this condition were homogeneous and transparent, which were named as BPAA-GFF-PC and BPAA-AFF-PC, respectively. All the nanofibers within BPAA-GFF-PC and BPAA-AFF-PC had a uniform width of 10 nm and contacted with each other closely, which were similar to the morphology of natural extracellular matrix (ECM). Rheology measurements were used to characterize the viscoelastic properties of the hydrogels. An amplitude sweep analysis (Figure 6B1) confirmed that the linear viscoelastic regime ($G' > G''$) was between 0.1 and 10%. For frequency sweep analysis (Fig. 6B2), the value of amplitude was chosen at 0.5%, within the linear viscoelastic regime. All of the hydrogels presented a weak frequency dependence, while the G' of BPAA-GFF-PC and BPAA-AFF-PC was around 5 kPa and 13.8 kPa, respectively. The time sweep analysis at room temperature (Fig. 6C1-C2) showed the gel state ($G' > G''$) at 0.5% strain and the liquid state of the hydrogels ($G' < G''$) at 100.0% amplitude. The viscoelastic properties of the hydrogels in simulated physiological condition were similar to the hydrogels formed at pH 7, indicating the dominant effect of the pH switch on the self-assembly process. The secondary structure of the supramolecular architecture was investigated using CD spectra, and the fluorescence spectroscopy was used to analyze the intermolecular arrangement of gelators. The data of CD spectra (Fig. 6D1-D2) illustrated that the supramolecular polymers generated in simulated physiological condition presented typical β-sheet self-assembling structure, while the fluorescence emission spectra (Fig. 6E1-E2) showed that the gelators within BPAA-AFF-PC hydrogel possessed stronger intermolecular actions, and could build more stable supramolecular arrangements and generate stiffer hydrogels, which agreed well with the rheological characteristics of the hydrogels.

In order to investigate the cytotoxicity of the materials, the gelators were co-cultured with L929 cells, and MTT assay was performed to evaluate the cells viability. Figure S5 showed that the cell viability of BPAA-FFG, BPAA-FFA, BPAA-GFF and BPAA-AFF were more than 75% after 24 h or 72 h culture, expressing good biocompatibility. The gelation time of BPAA-FFG and BPAA-FFA were about 2.5 h at concentration of 20 mM, which was not suitable for cell encapsulation. While the gelation time of BPAA-GFF and BPAA-AFF were less than 30 min with the same concentration, which was available for cell encapsulation. Thus, the morphology of L929 cells encapsulated in BPAA-GFF and BPAA-AFF were observed by CLSM after live-dead staining (FDA and PI stain) and SEM after critical point drying (Fig. 6F). The CLSM presented the variation of L929 cells profile from round in 1 day to spindle after 7 days culture, indicating the attachment of cell to the molecules in hydrogels. The cell viability test results revealed hydrogels were effective in maintaining cell spreading and proliferation. The SEM further showed the typical morphology of L929 cells with intensively adhesive on the hydrogels. In addition, the cell attachment and spreading within the hydrogels at 7 days were further detected by cytoskeletal F-actin staining using rhodamine-phalloidin. The CLSM pictures presented the highly elongated actin filaments (red) surrounding the nuclei (blue) of cells, which showed the obviously attached growth of L929 cells. To further confirm the proliferation of L929 cells in the hydrogels, the quantitative analysis was conducted using the MTT assay, and the results were displayed in Figure 6G1-G2. It was found that the absorbance at 490 nm increased in two experimental groups when the culture period was prolonged from 1 day to 7 days. This result meant a significant increase in cell population, showing the great proliferative potential of L929 cells in the hydrogels. This result was consistent with that from CLSM, SEM and live/dead staining assay.

3.7. Construction of engineered cartilage tissue in vitro

In this study, BPAA-GFF and BPAA-AFF formed under simulated physiological condition was utilized as scaffold to encapsulate chondrocytes and build 3D culture constructs. After cultured for 7, 14, and 21 days, the constructs were evaluated by CLSM observation after FDA and PI staining. As shown in Fig. 7A, the CLSM pictures showed that most of the chondrocytes remaining round shape were entrapped in the gel and almost no dead cells were detected, which revealed that the two hydrogels had good biocompatibility. Besides, the cell numbers increased with the prolongation of culture time and presented clustered growth from 7 days to 14 days. After 21 days of culture, the phenomenon that several chondrocytes grew in a cavitation could be observed, indicating the formation of cartilage lacuna structure. The morphology of chondrocytes/scaffold construct was also analyzed by SEM after 7, 14,

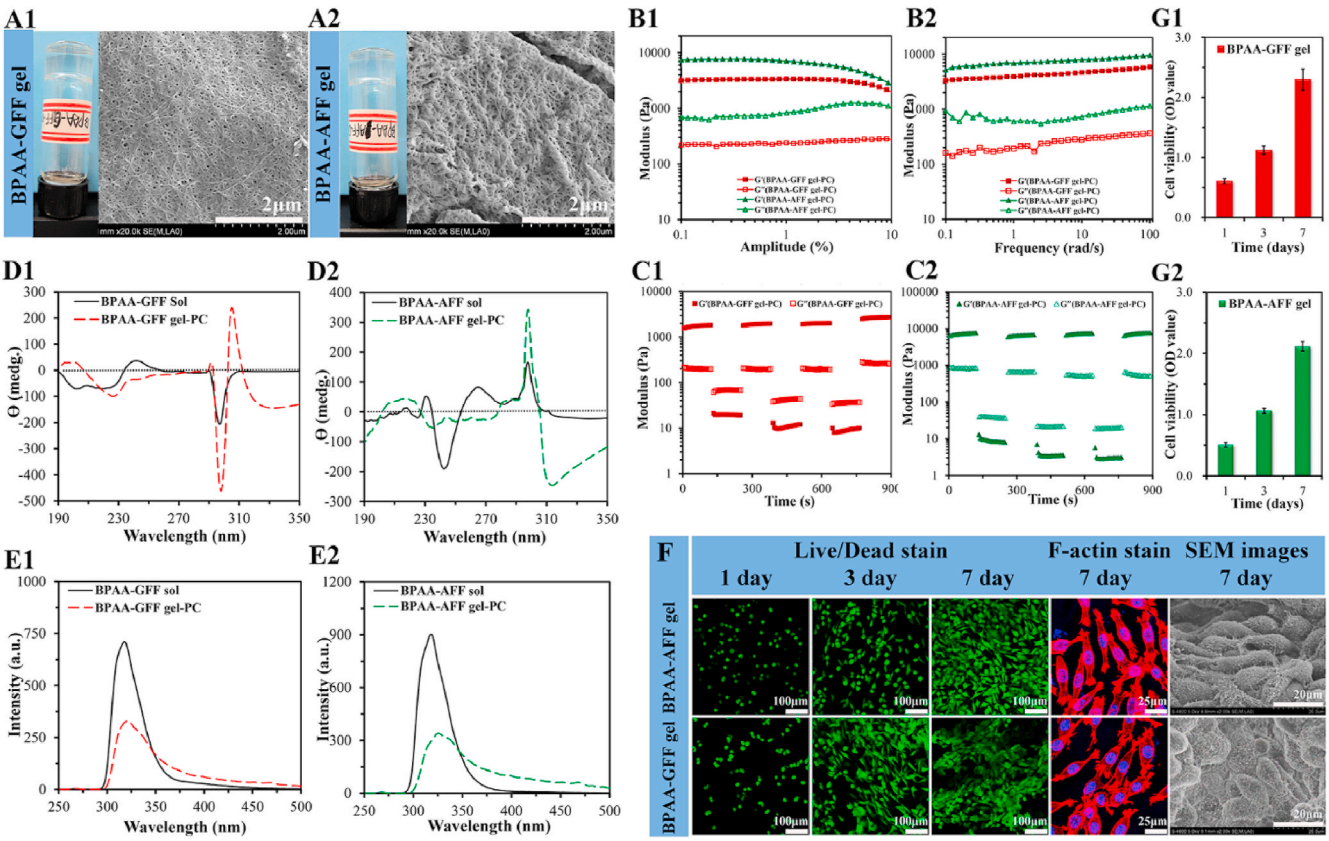

Fig. 6. (A) The optical images and SEM micrographs of the hydrogels prepared in simulated physiological condition (PC). (B1 and B2) Amplitude sweep analysis of hydrogels (Frequency = 1.0 Hz) and frequency sweep analysis of hydrogels (Strain = 0.5%). (C1 and C2) Time sweep analysis of hydrogels (Strain = 0.5% or 100%). (D1 and D2) CD spectra of Sol-GFF, Sol-AFF and Gel-GFF-PC, Gel-AFF-PC. (E1 and E2) Fluorescence emission spectra of Sol-GFF and Sol-AFF and Gel-GFF-PC, Gel-AFF-PC. (λexc = 265 nm). (F) CLSM images (FDA/PI staining) of L929 cells encapsulated into Gel-GFF-PC and Gel-AFF-PC, CLSM images (Rhodamine-phalloidin/Hoechst staining) of L929 cells encapsulated into Gel-GFF-PC and Gel-AFF-PC after 7 days incubation as well as SEM images of L929 cells encapsulated into Gel-GFF-PC and Gel-AFF-PC after 7 days incubation. (G1 and G2) The proliferation of L929 cells encapsulated into Gel-GFF-PC and Gel-AFF-PC during 7 days incubation.

21 days culture. The results indicated the typical round morphology of the chondrocytes in the growth process. When cultured from 7 days to 14 days, chondrocytes grew into cell cluster from single cells. After 21 days of culture, larger size chondrocytes cluster were observed. The image also demonstrated the ability of cell proliferation in the dense fiber of the type II collagen produced by the chondrocytes. This phenomenon illustrated that the proliferation of chondrocytes and cartilage lacuna formation, which was consistent with the results of CLSM. During the culture, chondrocytes secreted a large amount of extracellular matrix (ECM), predominantly containing collagen II and proteoglycan. Proteoglycan attached to collagen II molecules to form network structure, which played complimentary roles in the biomechanical behavior of articular cartilage. The results of Fig. 7B and C showed that the secretion of GAG and collagen II in the chondrocytes significantly increased with the prolongation of the culture time.

The further observation and analysis of the chondrocytes proliferation and the secretion of ECM was examined with histological staining after 7, 14 and 21 days. The chondrocytes/scaffold constructs were sectioned and stained with H&E to examine tissue organization, with SO to observe GAG synthesis, and with TB to detect proteoglycans (Fig. 7D). From H&E staining, clear staining of chondrocytes within lacunae was presented after 21 days of culture in two hydrogel. It showed that the chondrocytes gradually exhibited normal morphology of the natural cartilage tissue during culture. The SO and TB staining showed that there was more positive staining of polysaccharides (red and blue purple) in BPAA-AFF-PC/chondrocytes constructs when cultured for 7 days. The staining range expanded and the color gradually deepened with the extension of culture time, indicating that chondrocytes secreted more polysaccharides in BPAA-AFF-PC hydrogel during culture. From the immunohistochemical staining of Col II (Fig. 7D), it also could be seen that there was more positive staining (dark brown color) in BPAA-AFF-PC/chondrocytes constructs on the 7 day of culture, and the staining gradually deepened with the prolongation of culture time, indicating that chondrocytes could continually secrete more collagen II during culture versus BPAA-GFF-PC/chondrocytes constructs. Immunohistochemical staining showed that chondrocytes could play normal physiological functions and secrete more specific ECM of natural cartilage when encapsulated in three-dimensional supramolecular BPAA-AFF-PC hydrogel. The hydrogel/cell/matrix constructs after 21 days culturing in Fig. 7D exhibited the neo-matrix formation around chondrocytes in the hydrogels. The mechanical strength of constructs was examined by dynamic mechanical analysis (Fig. 7E–H). These results were shown as below, the storage and loss modulus of two hydrogels decreased after 21 days culturing. The underlying reason was that the degradation of hydrogels *in vitro* gradually led to structure dissociation. However, the storage modulus of all hydrogels was higher than that of loss modulus, indicating that gel maintenance might be due to synchronous formation of new matrix, which was consistent with the results of Fig. 7D. Meanwhile, the higher modulus of BPAA-AFF also implied better structural stability and tissue inductance.

In order to quantitatively analyze the level of two supramolecular hydrogels to maintain the normal physiological function of chondrocytes, relevant genes expression was detected, such as Collagen I (Col I), Collagen II (Col II), Collagen X (Col X), Aggrecan (AGG), SRY-related high mobility group box gene 9 (SOX9), using GAPDH as the housekeeper gene. Col II and AGG are the specific matrices of hyaline

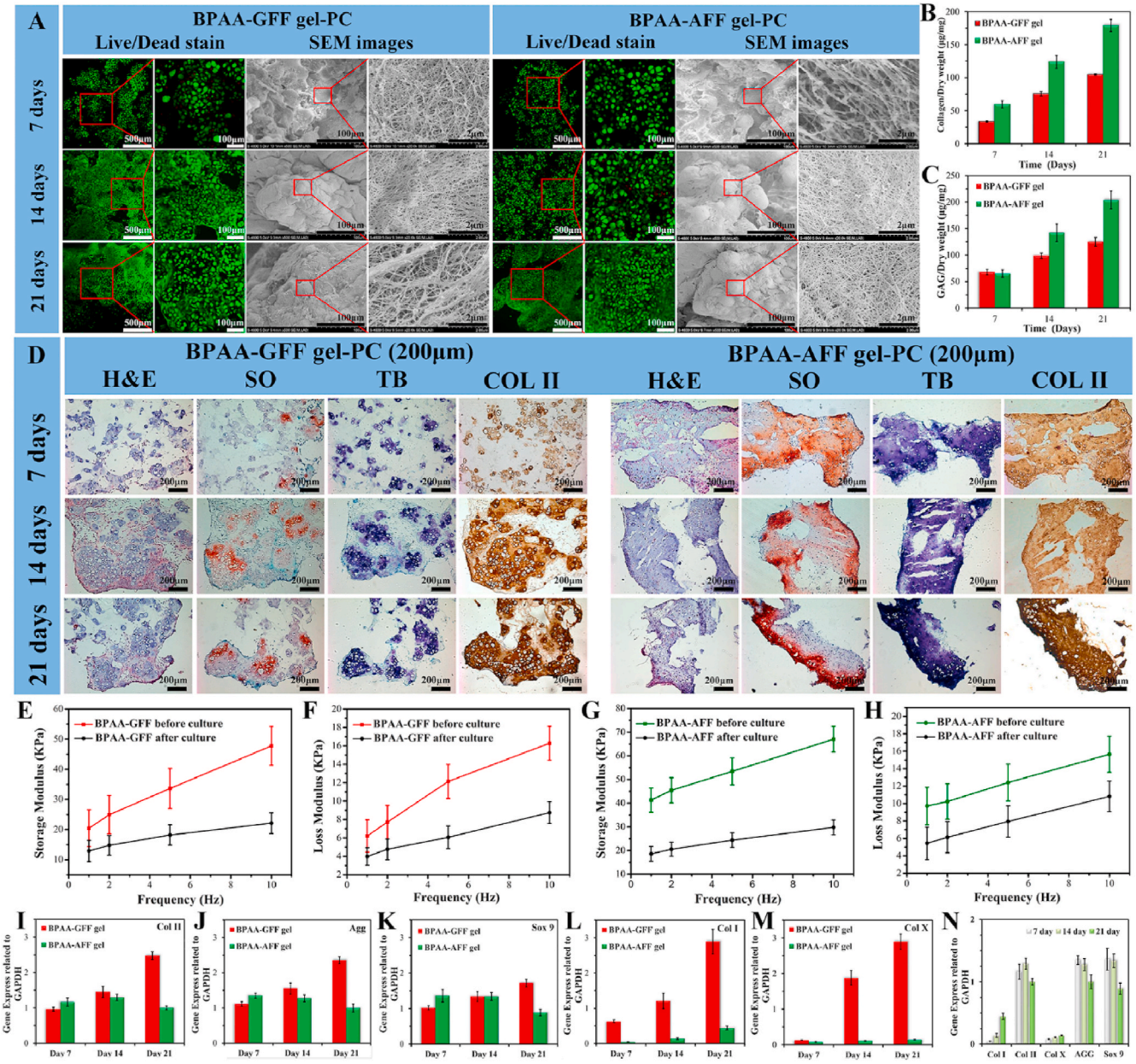

Fig. 7. (A) CLSM images (FDA/PI staining) and SEM images of chondrocytes encapsulated into Gel-GFF-PC and Gel-AFF-PC hydrogels. The GAG (B) and Collagen (C) contents related to the dry weight of chondrocyte/hydrogel constructions. (D) Histological analysis of cartilage-matrix related secretion by chondrocytes encapsulated in Gel-GFF-PC and Gel-AFF-PC hydrogels. (H&E = hematoxylin and eosin staining; SO = Safranin-O staining; TB = Toluidine blue staining; Col II = Immunohistochemical staining for type II collagen) (E–H) DMA analysis of hydrogels before and after culture *in vitro*. (I–M) qRT-PCR analysis disclosed the gene expression of cartilage-matrix related proteins by chondrocytes encapsulated in Gel-GFF-PC and Gel-AFF-PC hydrogels, including Col I, Col II, Col X, AGG and Sox 9. (N) Time-evolution of integral gene expression of cartilage-matrix related proteins by chondrocytes encapsulated in Gel-AFF-PC hydrogels. (For interpretation of the references to color in this figure legend, the reader is referred to the Web version of this article.)

cartilage; SOX9 is the chondrogenic phenotype marker; Col I is a maker related to cell adhesion, migration, dedifferentiation of chondrocytes and differentiation of osteoblasts; and Col X is the marker for the hypertrophy of chhondrocytes. As shown in Fig. 7I-N, Col II, AGG and SOX9 genes expression showed nearly no significant difference in BPAA-GFF-PC and BPAA-AFF-PC, but Col I and Col X genes expression in BPAA-AFF-PC was quite lower than that in BPAA-GFF-PC. In addition, the expression of chondrogenic marker genes Col II, AGG and SOX9 were significantly higher than those of the Col I and Col X in BPAA-AFF-PC. All these results suggested that BPAA-AFF-PC and BPAA-GFF-PC could maintain the normal physiological function of chondrocytes, and BPAA-AFF-PC had better performance in facilitating proliferation of chondrocytes, producing a hyaline cartilage rather than fibrous cartilage or ossification versus BPAA-GFF-PC. These findings implied that the BPAA-AFF-PC hydrogel was more suitable for long-term cartilage treatment.

4. Conclusion

Here, supramolecular nanofiber hydrogels based on biphenyl-tripeptides with different primary amino acid sequences were prepared and characterized. The minimum gelation concentration (MGC) was only 0.4 mM (0.022 wt%) by pH switch, and the maximum storage modulus was around 13.8 kPa in simulated physiological condition (pH = 7 and 0.01 M PBS). The morphology of the hydrogels was similar to that of natural extracellular matrix. The molecular dynamics simulations predicted that nanofibers self-assembly mainly depended on “FF” brick

and hydrogen bond interactions. The rheological analysis, CD, FT-IR, and spectroscopy further confirmed and optimized amino acid sequences. The supramolecular nanofiber hydrogels as 3D scaffold could effectively support chondrocytes and L929 cells spreading and proliferation. Histological and immunohistochemical staining showed that chondrocytes could perform normal physiological functions and secrete specific ECM. Quantitative PCR results indicated that chondrogenic marker genes expression level (Col II, AGG and SOX9) was up-regulated while hypertrophic cartilage genes expression level (Col I and Col X) was suppressed. These findings implied that biphenyl-tripeptide hydrogels hold great potential in regenerative medicine as promising innovative matrices.

CRediT authorship contribution statement

Yong Sun: Data curation, Formal analysis, Methodology, Software, Funding acquisition, Writing – original draft. **Xing Li:** Methodology, Software, Writing – review & editing. **Mingda Zhao:** Conceptualization, Writing – review & editing. **Yafang Chen:** Conceptualization, Writing – review & editing. **Yang Xu:** Conceptualization, Writing – review & editing. **Kefeng Wang:** Software, Formal analysis. **Shaoquan Bian:** Writing – review & editing, Conceptualization. **Qing Jiang:** Conceptualization. **Yujiang Fan:** Funding acquisition, Resources, Supervision, Writing – review & editing. **Xingdong Zhang:** Resources, Project administration.

Acknowledgements

This work was sponsored by National Key R&D Program of China (Grant No. 2018YFC1105900), National Natural Science Foundation of China (32071352), Sichuan Province Key R&D Program (2019YFS0007) and Sichuan university Innovation Spark Project (2018SCUH0089).

Appendix A. Supplementary data

Supplementary data to this article can be found online at https://doi.org/10.1016/j.bioactmat.2021.05.054.

Declaration of competing interest

The authors declare that they have no known competing financial interests or personal relationships that could have appeared to influence the work reported in this paper.

References

[1] J. Gačanin, J. Hedrich, S. Sieste, G. Glaßer, I. Lieberwirth, C. Schilling, S. Fischer, H. Barth, B. Knöll, C.V. Synatschke, T. Weil, Autonomous ultrafast self-healing hydrogels by pH responsive functional nanofiber gelators as cell matrices, Adv. Mater. 31 (2019) 1805044.
[2] C.G. Wang, M. Wang, K.S. Xia, J.K. Wang, F. Cheng, K.S. Shi, L.W. Ying, C. Yu, H. B. Xu, S.N. Xiao, C.Z. Liang, F.C. Li, B. Lei, Q.X. Chen, A bioactive injectable self-healing anti-inflammatory hydrogel with ultralong extracellular vesicles release synergistically enhances motor functional recovery of spinal cord injury, Bioact. Mater. 6 (2021) 2523–2534.
[3] Z.R. Jia, X.H. Lv, Y. Hou, K.F. Wang, F.Z. Ren, D.G. Xu, Q. Wang, K.L. Fan, C. M. Xie, X. Lu, Mussel-inspired nanozyme catalyzed conductive and self-setting hydrogel for adhesive and antibacterial bioelectronics, Bioact. Mater. 6 (2021) 2676–2687.
[4] Y. Wang, W.S. Zhang, C.C. Gong, B. Liu, Y.D. Li, L.C. Wang, Z.Q. Su, G. Wei, Recent advances in the fabrication, functionalization, and bioapplications of peptide hydrogels, Soft Matter 16 (2021) 10029–10045.
[5] L. Zhou, L. Fan, X. Yi, Z.N. Zhou, C. Liu, R.M. Fu, C. Dai, Z.G. Wang, X.X. Chen, P. Yu, D.F. Chen, G.X. Tan, Q.Y. Wang, C.Y. Ning, Soft conducting polymer hydrogels CrossLinked and doped by tannic acid for spinal cord injury repair, ACS Nano 12 (2018) 10957–10967.
[6] F. Wang, W. Ji, P. Yang, C.-L. Feng, Inversion of circularly polarized luminescence of nanofibrous hydrogels through coassembly with achiral coumarin derivatives, ACS Nano 13 (2019) 7281–7290.
[7] J.D. Tang, C. Mura, K.J. Lampe, Stimuli-responsive, pentapeptide, nanofiber hydrogel for tissue engineering, J. Am. Chem. Soc. 141 (2019) 4886–4899.
[8] M.C. Gómez-Guillén, B. Giménez, M.E. López-Caballero, M.P. Montero, Functional and bioactive properties of collagen and gelatin from alternative sources: a review, Food Hydrocolloids 25 (2011) 1813–1827.
[9] B. Trappmann, J.E. Gautrot, J.T. Connelly, D.G.T. Strange, Y. Li, M.L. Oyen, M. A. Cohen Stuart, H. Boehm, B. Li, V. Vogel, J.P. Spatz, F.M. Watt, W.T.S. Huck, Extracellular-matrix tethering regulates stem-cell fate, Nat. Mater. 11 (2012) 642–649.
[10] F.J. O'Brien, Biomaterials & scaffolds for tissue engineering, Mater. Today 14 (2011) 88–95.
[11] A.S. Hoffman, Hydrogels for biomedical applications, Adv. Drug Deliv. Rev. 64 (2012) 18–23.
[12] L. L Shang, Z.Q. Liu, B.J. Ma, J.L. Shao, B. Wang, C.X. Ma, S.H. Ge, Dimethyloxallyl glycine/nanosilicates-loaded osteogenic/angiogenic difunctional fibrous structure for functional periodontal tissue regeneration, Bioact, Mater 6 (2021) 1175–1188.
[13] Z.Y. Chen, Q. Zhang, H.M. Li, Q. Wei, X. Zhao, F.L. Chen, Elastin-like polypeptide modified silk fibroin porous scaffold promotes osteochondral repair, Bioact. Mater. 6 (2021) 589–601.
[14] M. Vázquez-González, I. Willner, Stimuli-ResponsiveBiomolecule-based hydrogels and their applications, Angew. Chem. Int. Ed. 59 (2020) 15342–15377.
[15] Z. Ye, X. Zhu, I. Mutreja, S.K. Boda, N.G. Fischer, A.Q. Zhang, C. Lui, Y. P Qi, C. Aparicio, Biomimetic mineralized hybrid scaffolds with antimicrobial peptides, Bioact. Mater. 6 (2021) 2250–2260.
[16] J. Cheng, D. Amin, J. Latona, E. Heber-Katz, P.B. Messersmith, Supramolecular polymer hydrogels for DrugInduced tissue regeneration, ACS Nano 13 (2019) 5493–5501.
[17] Y. Kuang, J.F. Shi, J. Li, D. Yuan, K.A. Alberti, Q.B. Xu, B. Xu, Pericellular hydrogel/nanonets inhibit cancer cells, Angew. Chem. Int. Ed. 53 (2014) 8104–8107.
[18] Y. Gao, J.F. Shi, D. Yuan, B. Xu, Imaging enzyme-triggered self-assembly of small molecules inside live cells, Nat. Commun. 3 (2012) 1033.
[19] W. Tanaka, H. Shigemitsu, T. Fujisaku, R. Kubota, S. Minami, K. Urayama, I. Hamachi, Post-assembly fabrication of a functional multicomponent supramolecular hydrogel based on a self-sorting double network, J. Am. Chem. Soc. 141 (2019) 4997–5004.
[20] M. Wang, J.Q. Wang, P. Zhou, J. Deng, Y.R. Zhao, Y.W. Sun, W. Yang, D. Wang, Z. Y. Li, X.Z. Hu, S.M. King, S.E. Rogers, H. Cox, T.A. Waigh, J. Yang, J.R. Lu, H. Xu, Nanoribbons self-assembled from short peptides demonstrate the formation of polar zippers between β-sheets, Nat. Commun. 9 (2018) 5118.
[21] J.L. Tan, M. Zhang, Z.J. Hai, C.F. Wu, J. Lin, W. Kuang, H. Tang, Y.L. Huang, X. D. Chen, G.L. Liang, Sustained release of two bioactive factors from supramolecular hydrogel promotes periodontal bone regeneration, ACS Nano 13 (2019) 5616–5622.
[22] B.W. Zhao, N.K. Li, Y.G. Yingling, C.K. Hall, LCST behavior is manifested in a single molecule: elastin-like polypeptide (VPGVG)n, Biomacromolecules 17 (2015) 111–118.
[23] P.W.J.M. Frederix, G.G. Scott, Y.M. Abul-Haija, D. Kalafatovic, C.G. Pappas, N. Javid, N.T. Hunt, R.V. Ulijn, T. Tuttle, Exploring the sequence space for (tri-) peptide self-assembly to design and discover new hydrogels, Nat. Chem. 7 (2014) 30–37.
[24] D.J. Adams, M.F. Butler, W.J. Frith, M. Kirkland, L. Mullen, P. Sanderson, A new method for maintaining homogeneity during liquid–hydrogel transitions using low molecular weight hydrogelators, Soft Matter 5 (2009) 1856.
[25] S. Fleming, S. Debnath, P.W.J.M. Frederix, T. Tuttle, R. V Ulijn, Aromatic peptide amphiphiles: significance of the Fmoc moiety, Chem. Commun. 49 (2013) 10587.
[26] D.J. Adams, L.M. Mullen, M. Berta, L. Chen, W.J. Frith, Relationship between molecular structure, gelation behaviour and gel properties of Fmoc-dipeptides, Soft Matter 6 (2010) 1971.
[27] C. Tang, R.V. Ulijn, A. Saiani, Effect of Glycine substitution on fmoc–diphenylalanine self-assembly and gelation properties, Langmuir 27 (2011) 14438.
[28] T.D. Schneider, R.M. Stephens, Sequence logos - a new way to display consensus sequences, Nucleic Acids Res. 18 (1990) 6097–6100.
[29] G.E. Crooks, G. Hon, J.M. Chandonia, S.E. Brenner, WebLogo: a sequence logo generator, Genome Res. 14 (2004) 1188–1190.
[30] X. Li, Y. Gao, Y. Kuang, B. Xu, Enzymatic formation of a photoresponsive supramolecular hydrogel, Chem. Commun. (Camb). 46 (2010) 5364.
[31] S.J. Lee, E. Kim, M.L. Seo, Y. Do, Y.A. Lee, S.S. Lee, J.H. Jung, M. Kogiso, T. Shimizu, Self-assembled helical ribbon and tubes of alanine-based amphiphiles induced by two different formation mechanisms, Tetrahedron 64 (2008) 1301.
[32] A.M. Castilla, M. Wallace, L.L.E. Mears, E.R. Draper, J. Doutch, S. Rogers, D. J. Adams, On the syneresis of an OPV functionalised dipeptide hydrogel, Soft Matter 12 (2016) 7848.
[33] I.P. Moreira, I.R. Sasselli, D.A. Cannon, M. Hughes, D.A. Lamprou, T. Tuttle, R. V Ulijn, Enzymatically activated emulsions stabilized by interfacial nanofibre networks, Soft Matter 12 (2016) 2623.
[34] Z. Yang, H. Gu, Y. Zhang, L. Wang, B. Xu, Small molecule hydrogels based on a class of antiinflammatory agents, Chem. Commun. (Camb). 2 (2004) 208.
[35] Z. Yang, H. Gu, D. Fu, P. Gao, J.K. Lam, B. Xu, Enzymatic formation of supramolecular hydrogels, Adv. Mater. 16 (2004) 1440.
[36] A.M. Smith, R.J. Williams, C. Tang, P. Coppo, R.F. Collins, M.L. Turner, A. Saiani, R.V. Ulijn, Fmoc-diphenylalanine self assembles to a hydrogel via a novel architecture based on π–π interlocked β-sheets, Adv. Mater. 20 (2008) 37.
[37] J.P. Perdew, K. Burke, M. Ernzerhof, Generalized gradient approximation made simple, Phys. Rev. Lett. 77 (1996) 3865–3868.

[38] L. Kale, R. Skeel, M. Bhandarkar, R. Brunner, A. Gursoy, N. Krawetz, J. Phillips, A. Shinozaki, K. Varadarajan, K. Schulten, Namd2: greater scalability for parallel molecular dynamics* 1, J. Comput. Phys. 151 (1999) 283–312.
[39] J. Huang, S. Rauscher, G. Nawrocki, T. Ran, M. Feig, B.L. de Groot, H. Grubmüller, A.D. MacKerell, Charmm36m: an improved force field for folded and intrinsically disordered proteins, Nat. Methods 14 (2017) 71–73.
[40] W.L. Jorgensen, J. Chandrasekhar, J.D. Madura, R.W. Impey, M.L. Klein, Comparison of simple potential functions for simulating liquid water, J. Chem. Phys. 79 (1983) 926.
[41] J. Shen, T. Wu, Q. Wang, H. Pan, Molecular simulation of protein adsorption and desorption on hydroxyapatite surfaces, Biomaterials 29 (2008) 513–532.
[42] Y. Kang, X. Li, Y. Tu, Q. Wang, H. Agren, On the mechanism of protein adsorption onto hydroxylated and nonhydroxylated Tio2 surfaces, J. Phys. Chem. C 114 (2010) 14496–14502.
[43] W.M. Dawson, F.J.O. Martin, G.G. Rhys, K.L. Shelley, R.L. Brady, D.N. Woolfson, Coiled coils 9-to-5: rational de novo design of alpha-helical barrels with tunable oligomeric states, Chem. Sci. (2021).
[44] A.M. Smith, R.J. Williams, C. Tang, P. Coppo, R.F. Collins, M.L. Turner, A. Saiani, R.V. Ulijn, Fmoc-diphenylalanine self assembles to a hydrogel via a novel architecture based on π-π interlocked β-sheets, Adv. Mater. 20 (1) (2008) 37–41.
[45] B. Jeong, Y.H. Bae, S.W. Kim, Thermoreversible gelation of PEG-PLGA- PEG triblock copolymer aqueous solutions, Macromolecules 32 (21) (1999) 7064–7069.
[46] H.D.T. Mertens, D.I. Svergun, Structural characterization of proteins and complexes using small-angle X-ray solution scattering, J. Struct. Biol. 172 (1) (2010) 128–141.
[47] D.J. Segel, A.L. Fink, K.O. Hodgson, S. Doniach, Protein denaturation: a small-angle X-ray scattering study of the ensemble of unfolded states of cytochrome c, Biochemistry 37 (36) (1998) 12443–12451.
[48] D.W. Schaefer, K.D. Keefer, Structure of random porous materials: Silicaaerogel, Phys. Rev. Lett. 56 (20) (1986) 2199–2202.